Chinese Chemical Letters 37 (2026) 112050

Contents lists available at ScienceDirect

Chinese Chemical Letters

journal homepage: www.elsevier.com/locate/cclet

Metal-free carbon quantum dots as photocatalyst for phosphonation of undirected heteroaryl compounds

Tong Yue[a], Jun-Bo Wang[a], Xin-Yue Wang[a], Ming-Yi Huang[a], Mo Zhang[b,*], Zhan-Hui Zhang[a,*]

[a] Hebei Key Laboratory of Organic Functional Molecules, College of Chemistry and Materials Science, Hebei Normal University, Shijiazhuang 050024, China
[b] School of Pharmacy, Key Laboratory of Innovative Drug Development and Evaluation, Hebei Medical University, Shijiazhuang 050017, China

ARTICLE INFO

Article history:
Received 23 July 2025
Revised 23 October 2025
Accepted 31 October 2025
Available online 3 November 2025

Keywords:
Photocatalysis
Carbon dots
Cross-dehydrogenative coupling reaction
Phosphinoylation
2-Methyl tetrahydrofuran

ABSTRACT

Nitrogen-doped carbon dots (N-CDs) were synthesized *via* a hydrothermal method, utilizing citric acid and urea as precursor materials. Through a systematic characterization and evaluation process, the N-CDs variant with the highest amino group density was identified as an outstanding metal-free photocatalyst. Under ambient conditions, this photocatalyst exhibited remarkable catalytic performance in promoting visible-light-driven cross-dehydrogenative coupling (CDC) reactions between heteroaryl substrates and a wide range of H-phosphine oxide derivatives. This methodology presents several noteworthy advantages, such as operational stability and recyclability of the photocatalyst system, compatibility with various functional groups, mild reaction parameters, scalability for practical applications, and eco-friendly implementation using a mixed solvent system composed of 2-methyl tetrahydrofuran (2-Me THF) and water as the solvent medium. The developed protocol demonstrates enhanced process sustainability through its combination of environmental benignity and technical practicality.

© 2026 Published by Elsevier B.V. on behalf of Chinese Chemical Society and Institute of Materia Medica, Chinese Academy of Medical Sciences.

The traditional methods for construction of C-P bond are mainly based on transition-metal-mediated cross-coupling of boric acid [1], aryl halides [2], diaryliodonium salts [3], aryl nonaflates [4], aromatic esters [5], triarylbismuths [6], fluorosulfonates [7], arylsilanes [8] or aroylhydrazides [9] with organophosphorus creagents using palladium, nickel, or copper catalysts with air-sensitive ligands. However, these conventional protocols exhibit critical limitations including substrate prefunctionalization requirements, costly noble metal catalysts, and sophisticated ligand systems, which significantly restrict their practical applicability in synthetic chemistry. Innovative strategies focusing on transition metal-free cross-dehydrogenative coupling (CDC) systems have emerged as viable alternatives, particularly the direct functionalization of heteroarenes with phosphite esters under metal-free conditions. This methodology circumvents prerequisite substrate activation, enabling direct C-H phosphonation through radical intermediates while preserving native functional groups [10]. Recent advances demonstrate that heteroaromatic frameworks containing electron-rich heterocycles (*e.g.*, dibenzothiazepines, quinoxalinones, and pyrrolopyrimidines) can serve as efficient phosphonation substrates when activated by stoichiometric metal oxidants (*e.g.*, $Mn(OAc)_3$ or $K_2S_2O_8$) under thermal conditions [11–18]. The operational efficiency of these transformations critically depends on the formation of stabilized cationic intermediates, which undergo rapid phosphorylation with nucleophilic phosphorus species.

The heteroaryl compounds containing a furan or thiophene nucleus are widely found in natural products and pharmaceutical drugs [19–21]. The introduction of a phosphoryl group onto a heteroaryl skeleton can strengthen its bioactivities. Heteroaryl phosphorus compounds are also very important functional molecules widely used in diverse fields, such as drugs, advanced functional materials, agricultural chemistry, organic synthesis or even as ligands in catalysis (Fig. 1) [22–28]. Because of their extensive application, great efforts have been executed to develop efficient synthetic strategies for introducing the phosphonate esters into these heteroaryl skeleton [29]. In 2006, Zhang's group reported direct phosphonation of thiazoles, furans, and pyrroles in the presence of 3 equiv. of $Mn(OAc)_3{\cdot}2H_2O$ in acetic acid at 80 °C (Scheme 1A) [30]. Afterward, several reports have been published using Cu(I)/Cu(II) as catalyst and $K_2S_2O_8$ as oxidant (Scheme 1B) [31] and catalytic $Mn(OAc)_2$/excess MnO_2 system (Scheme 1C) [32] for this kind of transformation. Lei *et al.* has also introduced a Mn-catalyzed electrooxidative dehydrogenative C-H/P-H cross-coupling between electron-rich aromatics and phosphine oxides (Scheme 1D) [33].

* Corresponding authors.
E-mail addresses: 19101691@hebmu.edu.cn (M. Zhang), zhanhui@hebtu.edu.cn (Z.-H. Zhang).

https://doi.org/10.1016/j.cclet.2025.112050
1001-8417/© 2026 Published by Elsevier B.V. on behalf of Chinese Chemical Society and Institute of Materia Medica, Chinese Academy of Medical Sciences.

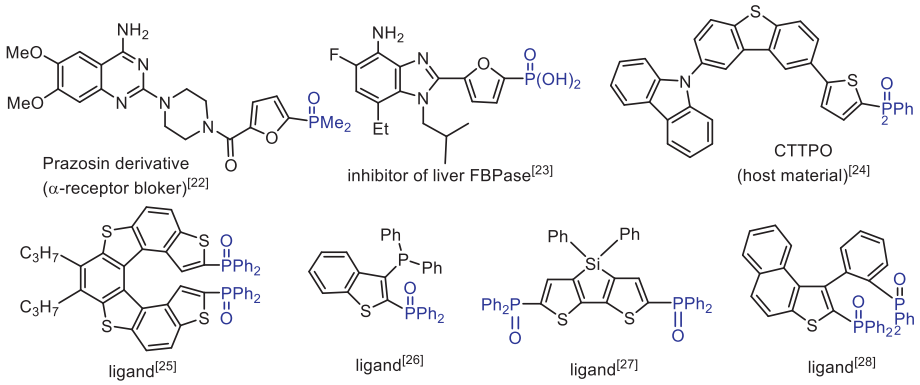
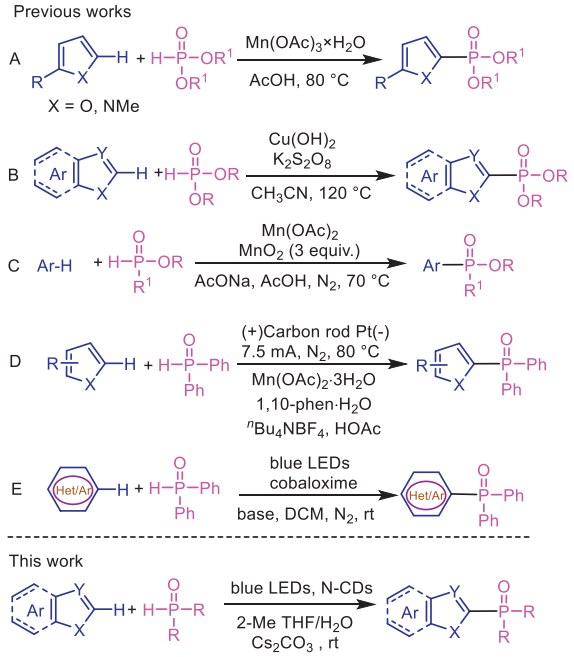
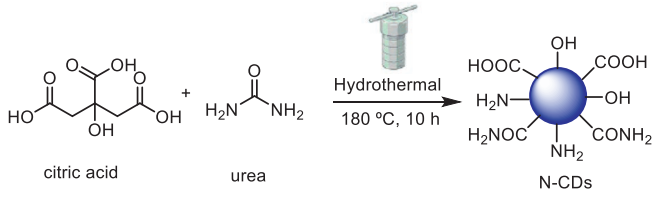


Fig. 1. Representative examples with phosphoryl group.



Scheme 1. The reported strategies and the present work for phosphonation of undirected heteroaryl compounds.



Scheme 2. Synthesis of N-CDs using citric acid and urea.

In recent times, the employment of the visible light-induced catalytic system has been demonstrated as a more favorable option for achieving transition metal-catalyzed C-H phosphorylation under mild circumstances [34–37]. In 2022, visible light-induced cobaloxime ($Co(dmgH)_2Cl_2$) catalyze the phosphinoylation of undirected heterocycles in a nitrogen atmosphere in dichloromethane (DCM) was reported. (Scheme 1E) [38,39]. However, notwithstanding these advancements, these methods still fall short of meeting the criteria of green chemistry. This is mainly because of the utilization of high-cost transition metal catalyst and the highly toxic DCM solvent. From the perspective of environmental friendliness, it would be highly desirable to devise an environmentally benign method for constructing the C-P bond.

Owing to their distinctive physicochemical characteristics, including exceptional specific surface area, tunable porosity, superior electrical conductivity, facile synthesis and functionalization, cost-effectiveness, and environmental compatibility, carbon-based materials have emerged as promising alternatives to conventional metal catalysts in various chemical processes [40–42]. Among these materials, carbon quantum dots (CQDs), a class of zero-dimensional carbon nanomaterials with particle sizes typically below 10 nanometers, have garnered significant attention in multidisciplinary applications. Their unique combination of properties, such as abundant precursor availability, tunable photoluminescence, remarkable quantum yield, excellent aqueous dispersibility, outstanding photostability, and favorable biocompatibility, has enabled their widespread utilization in diverse fields including biomedical imaging, optoelectronic devices, chemical sensing, and catalytic applications [43–48]. Particularly noteworthy is their role as efficient photosensitizers in visible-light-mediated organic transformations, demonstrating their potential in sustainable chemical synthesis [49–61]. In addition, 2-methyl tetrahydrofuran (2-Me THF) derived from biomass feedstocks, is a safe and low-toxic solvent with good stability to acids and bases. Building upon our recent explorations into sustainable synthetic methodologies [62–67] and considering the current scientific context, a novel photocatalytic application of nitrogen-doped carbon dots (N-CDs) was demonstrated as an efficient catalyst for direct C-P bond formation on diverse heteroaryl frameworks under mild conditions. The reaction system employed a mixed solvent composed of 2-methyltetrahydrofuran (2-Me THF) and water at room temperature, achieving high selectivity for undirected heteroaromatic substrates without requiring directing groups or external oxidants (Scheme 1).

Nitrogen doped carbon dots (N-CDs) were constructed by the hydrothermal method with citric acid and urea as raw materials. The synthesis process of N-CDs is shown in Scheme 2.

To rigorously characterize the chemical functionalities of N-CDs, complementary surface analytical techniques were employed, including Fourier transform infrared spectroscopy (FT-IR) and X-ray photoelectron spectroscopy (XPS). The FT-IR spectrum of N-CDs (Fig. 2) revealed characteristic absorption features spanning the wavenumber range of 400–4000 cm^{-1}, indicative of diverse surface functional groups. A broad absorption band at 3237 cm^{-1} corresponds to O-H/N-H stretching vibrations, commonly observed in hydroxyl (-OH) and amine (-NH) moieties. A sharp peak at 1673 cm^{-1} is attributed to C=O stretching vibrations in amide (-CONH-) groups, originating from citric acid-urea condensation. Supplementary evidence of amide bond formation includes an in-

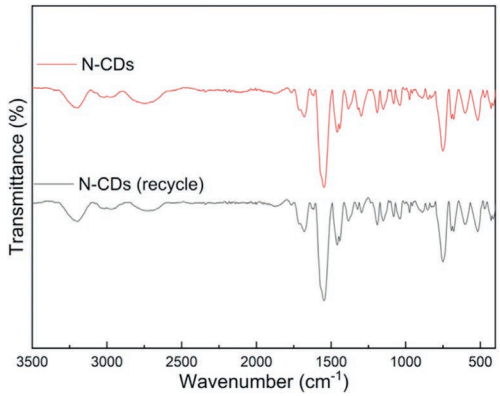


Fig. 2. FTIR spectra of N-CDs (fresh and recycled).

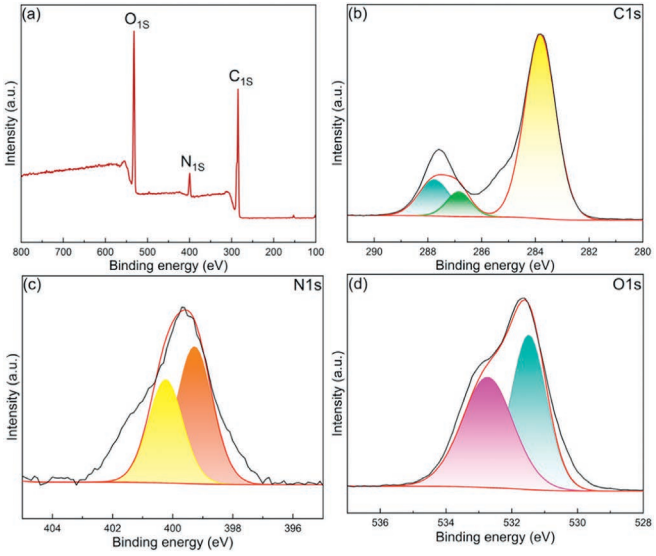


Fig. 3. High-resolution XPS spectra of the N-CDs: (a) Overall XPS spectrum, (b) C 1s XPS spectra, (c) N 1s XPS spectra, and (d) O 1s XPS spectra.

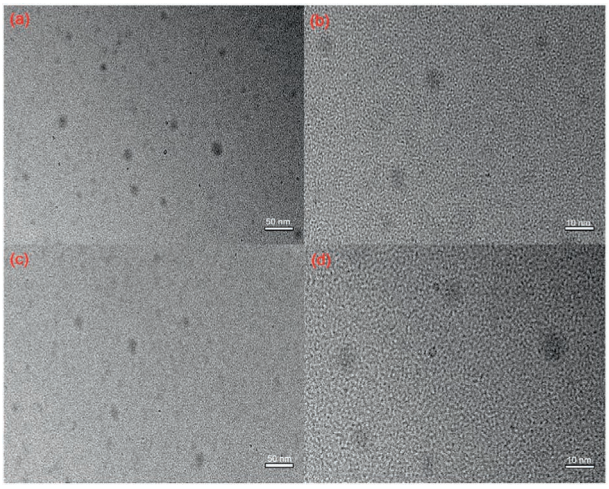


Fig. 4. TEM image of the N-CDs (fresh and recycled).

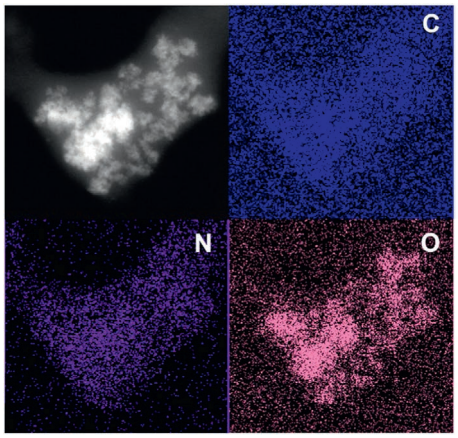


Fig. 5. Mapping spectra of the N-CDs.

plane N-H bending vibration at 1541 cm^{-1} and characteristic C=O stretching vibrations within the 1640–1680 cm^{-1} range, consistent with secondary amide structures. The retention of amide bond integrity post-recovery is confirmed by the absence of significant peak intensity shifts, underscoring structural stability of the synthesized N-CDs. The C-N stretching vibration in the amide linkage was identified at 1443 cm^{-1}, while the band at 1074 cm^{-1} corresponds to C-O-C stretching, indicating ether bond formation through secondary cross-linking reactions. These groups not only stabilize the dispersion of quantum dots, but also can be used as active sites to adsorb reactants and reduce the activation energy of the reaction through coordination or hydrogen bonding.

The surface chemical composition and bonding states of N-CDs were systematically investigated using XPS (Fig. 3). The survey spectrum (Fig. 3a) confirmed the predominant elemental constituents of carbon (C 1s), nitrogen (N 1s), and oxygen (O 1s). High-resolution deconvolution of the C 1s core level spectrum (Fig. 3b) revealed three distinct components. The peak at 283.82 eV corresponds to hybrid carbon (C=C/C-C), suggesting a graphitized core structure in the nitrogen-doped carbon dots. The peak at 286.85 eV is attributed to the C-N bond, originating from the amide bond (-CONH-) formed by the condensation of residual hydroxyl groups in citric acid or urea. The peak at 287.77 eV is assigned to the C=O bond (-COOH) in carboxylic acid or carbonyl groups, confirming the presence of surface carboxylic acid groups. The N 1s spectrum (Fig. 3c) exhibited a bimodal distribution corresponding to two distinct nitrogen species. The N 1s spectrum (Fig. 3c) exhibited a bimodal structure. The peak at 399.28 eV corresponds to pyridine nitrogen (C-N-C), indicating successful embedding of nitrogen atoms into the six-membered ring of the carbon core, which can modulate the electronic energy band structure. The peak at 400.23 eV is attributed to amino groups (-NH) or pyrrole nitrogen (C=N). O 1s deconvolution (Fig. 3d) resolved two components at 531.48 eV (C=O) and 532.73 eV (C-O), corresponding to carboxylic acid/carbonyl oxygen and hydroxyl/ether bond oxygen, respectively, consistent with the C 1s results. The combined FT-IR and XPS analyses confirm the successful formation of an aromatic sp^2 carbon network in the N-CDs.

The morphological features, size distribution, and structural uniformity of N-CDs were characterized by transmission electron microscopy (TEM, Fig. 4). The micrographs reveal monodisperse, spherical nanoparticles with uniform dispersion and no detectable aggregation. Quantitative size analysis (Fig. 4b) indicates a narrow size distribution with an average size below 10 nm, confirmed by log-normal fitting of the size distribution histogram. Energy-dispersive X-ray spectroscopy (EDS) elemental mapping (Fig. 5) confirms uniform spatial distribution of constituent elements: Carbon (C) forms the primary matrix with homogenous intensity distribution, nitrogen (N) is primarily localized at core regions, indicative of graphitic nitrogen doping, oxygen (O) exhibits peripheral enrichment, correlating with surface functional groups.

The thermal decomposition behavior of N-CDs was systematically investigated through thermogravimetric analysis (TGA) under nitrogen atmosphere (Fig. S1 in Supporting information). The TGA profile exhibited a multi-step thermal decomposition pattern with distinct mass loss stages (20–900 °C), revealing the composite nature of the carbon-nitrogen matrix. In the temperature range of 20–120 °C, an approximate weight loss of ~2 % was observed, which is ascribed to removal of adsorbed moisture from surface hydroxyl groups. The second weight loss stage, occurring at 120–300 °C with a 20 % mass loss, is primarily due to the thermal dissociation of oxygen/nitrogen functional groups (such as carboxyl, hydroxyl, and amino) on the surface. These functional groups are introduced during the hydrothermal synthesis process through the condensation reaction of urea and citric acid. Their thermal stability is lower than that of the carbon skeleton, resulting in the precedence of decarboxylation or deamination reactions. The third stage of weight loss, which takes place at 300–500 °C with about 30 % mass loss, corresponds to the gradual oxidation of the sp^2/sp^3 hybrid carbon-based skeleton and the structural collapse of nitrogen doping sites (such as pyridine nitrogen and graphitic nitrogen). The fourth stage of slow weight loss, occurring at 500–800 °C with about 15 % mass loss, is associated with the transformation of residual amorphous carbon into a more stable graphite phase. This transformation is accompanied by trace carbon oxidation and ash residue formation, with the final carbon residue rate being approximately 35 %. These findings indicate that the N-CDs as a target material possess thermal stability up to near 200 °C.

The X-ray diffraction (XRD) pattern of N-CDs (Fig. S2 in Supporting information) exhibits a broad diffraction peak at $2\theta = 25.5°$, corresponding to a crystal plane spacing of 3.5 Å. This spacing matches the (002) plane of graphite carbon, confirming the formation of an sp^2-hybridized carbon framework as the primary structural component. Notably, the experimental peak position demonstrates a negative shift of about 1° relative to the ideal graphite (002) plane (~26.5°), which can be attributed to two synergistic effects: Local lattice distortion caused by nitrogen atom doping and interlayer spacing expansion induced by the embedding of amino functional groups (from urea decomposition) into the carbon matrix. The pronounced peak broadening characteristics indicate two concurrent structural features: High defect density within the carbon lattice resulting from nitrogen incorporation and quantum confinement effects characteristic of nanoscale dimensions. These structural features align with the typical physicochemical properties of quantum dot materials, suggesting the coexistence of crystalline order and nanoscale disorder in the N-CDs structure.

The optical properties of N-CDs were systematically investigated through UV–vis diffuse reflectance spectroscopy (DRS) and photoluminescence (PL) spectroscopy. The UV–vis absorption profile (Fig. S3 in Supporting information) exhibits three distinct absorption bands: A weak shoulder peak at 253 nm), assignable to $\pi-\pi^*$ transitions in sp^2-hybridized aromatic domains; a broad absorption band spanning 300–550 nm, corresponding to $n\rightarrow\pi^*$ transitions in carbonyl groups; a surface plasmon resonance feature at 620 nm, indicative of localized surface charge oscillations. Accordingly, the optical band gap energy is estimated to be 2.04 eV based on the Tauc plots calculated from the UV–vis DRS data (Fig. S4 in Supporting information).

Fig. 6 presents the photoluminescence (PL) spectra of N-CDs across an excitation wavelength range of 300–480 nm. As shown, N-CDs exhibit distinct excitation wavelength-dependent fluorescence characteristics. When the excitation wavelength gradually increases from 300 nm to 480 nm, the intensity of the fluorescence emission peak reaches a maximum at 400 nm and then gradually decreases as the excitation wavelength further redshifts beyond this point. Notably, under 400 nm excitation, the strongest photoluminescence emission is observed at 480 nm.

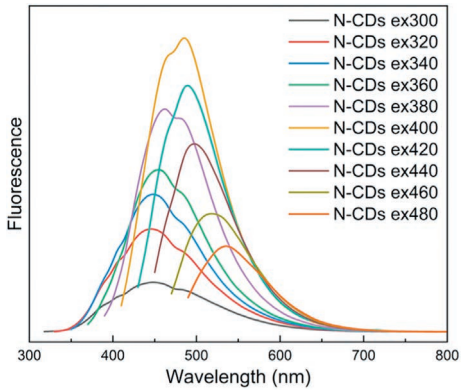
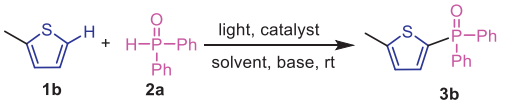


Fig. 6. Emission diagrams of the N-CDs with increasing excitation wavelengths from 300 nm to 480 nm in 20 nm increments.

Consequently, N-CDs were applied in the phosphinoylation reaction. To the best of our knowledge, the utilization of carbon dots as photocatalysts for the phosphinoylation of non-directed heteroaryl compounds has not been reported previously. Hence, we sought to explore their catalytic potential in this reaction. 2-Methylthiophene (**1b**) and diphenylphosphine oxide (**2a**) were selected as model substrates to optimize the reaction conditions (Table 1). A series of common solvents were screened under ambient temperature and blue light irradiation, with Cs_2CO_3 serving as the base. When CH_3CN or DMSO was used as the solvent, the reaction yields were low; in contrast, 2-Me THF enabled the formation of the product with a reasonable efficiency. To further enhance the reaction efficiency, a mixed solvent system of 2-Me THF and H_2O was investigated. Through subsequent optimization, employing a 2-Me THF/H_2O (1/3) mixed solvent increased the yield of **3b** to 85 % (Table 1, entry 14). The introduction of water increases the solubility of Cs_2CO_3, thus promoting the reaction. Subsequently, various bases were evaluated (entries 15−23). The results indicated that substituting Cs_2CO_3 with other bases led to a decrease in the yield of **3b** Screening different light sources revealed that a blue LED (450 nm) was the most effective for this reaction (entries 24−26). This phenomenon can be attributed to the energy band compatibility between the blue light and N-CDs; the energy of blue light aligns with the band gap (or surface state energy level) of N-CDs, facilitating efficient electron excitation to the conduction band and driving the photocatalytic reaction. Control experiments demonstrated that the reaction did not occur in the absence of a photocatalyst or under dark conditions (entries 27 and 28). Additionally, reducing the catalyst amount resulted in decreased reaction efficiency (entry 29), and shortening the reaction time to 12 h led to a lower yield of **3b** (entry 31). Other potential photocatalysts, including 4-CzIPN, CdS, $FeCl_3$, eosin B, rhodamine B, rose bengal, rhodamine 6G, and basic fuchsin, were also tested. However, none of them outperformed N-CDs in promoting the formation of the target product **3b** (entries 32–39).

Once the optimal reaction conditions were established (Table 1, entry 14), the proposed photocatalytic methodology embarked to explore the substrate scope of heteroaryl compounds for the synthesis of heteroaryl phosphorus compounds. As vividly depicted in Scheme 3, various substituted thiophene derivatives, whether adorned with electron-donating or electron-withdrawing groups, eagerly reacted with diphenylphosphine oxide to give the desired products (**3b**-**3g**) with yields ranging from moderate to rather impressive. Interestingly, halogen groups (-F, -Cl, and -Br) on the thiophene ring turned out to be the easy-going guests of this chemical party. They were well-tolerated by the reaction conditions, which provides a possibility for further modification at those halogenated positions through classical cross-coupling reactions. Notably, when

Table 1
Optimization of the reaction conditions for synthesis of **3a**.[a]



1b 2a 3b

Entry	Photocatalyst	Solvent	Base	Time (h)	Yield (%)[b]
1	N-CDs	EtOH	Cs_2CO_3	24	Trace
2	N-CDs	CPME	Cs_2CO_3	24	Trace
3	N-CDs	PEG 400	Cs_2CO_3	24	Trace
4	N-CDs	EL	Cs_2CO_3	24	Trace
5	N-CDs	DMF	Cs_2CO_3	24	8
6	N-CDs	EtOAc	Cs_2CO_3	24	15
7	N-CDs	Acetone	Cs_2CO_3	24	22
8	N-CDs	CH_3CN	Cs_2CO_3	24	32
9	N-CDs	DMSO	Cs_2CO_3	24	33
10	N-CDs	THF	Cs_2CO_3	24	35
11	N-CDs	H_2O	Cs_2CO_3	24	40
12	N-CDs	CH_2Cl_2	Cs_2CO_3	24	47
13	N-CDs	2-Me THF	Cs_2CO_3	24	70
14	N-CDs	2-Me THF/H_2O	Cs_2CO_3	24	85
15	N-CDs	2-Me THF/H_2O	$NaHCO_3$	24	Trace
16	N-CDs	2-Me THF/H_2O	Na_2CO_3	24	Trace
17	N-CDs	2-Me THF/H_2O	KOH	24	19
18	N-CDs	2-Me THF/H_2O	K_3PO_4	24	36
19	N-CDs	2-Me THF/H_2O	K_2CO_3	24	41
20	N-CDs	2-Me THF/H_2O	DABCO	24	20
21	N-CDs	2-Me THF/H_2O	DBU	24	33
22	N-CDs	2-Me THF/H_2O	Et_3N	24	39
23	N-CDs	2-Me THF/H_2O	Pyridine	24	43
24[c]	N-CDs	2-Me THF/H_2O	Cs_2CO_3	24	38
25[d]	N-CDs	2-Me THF/H_2O	Cs_2CO_3	24	42
26[e]	N-CDs	2-Me THF/H_2O	Cs_2CO_3	24	61
27[f]	N-CDs	2-Me THF/H_2O	Cs_2CO_3	24	Trace
28	No	2-Me THF/H_2O	Cs_2CO_3	36	Trace
29[g]	N-CDs	2-Me THF/H_2O	Cs_2CO_3	24	47
30[h]	N-CDs	2-Me THF/H_2O	Cs_2CO_3	24	85
31	N-CDs	2-Me THF/H_2O	Cs_2CO_3	12	48
32	4-CzIPN	2-Me THF/H_2O	Cs_2CO_3	24	11
33	CdS	2-Me THF/H_2O	Cs_2CO_3	24	21
34	$FeCl_3$	2-Me THF/H_2O	Cs_2CO_3	24	23
35	Eosin B	2-Me THF/H_2O	Cs_2CO_3	24	32
36	Rhodamine B	2-Me THF/H_2O	Cs_2CO_3	24	37
37	Rose Bengal	2-Me THF/H_2O	Cs_2CO_3	24	35
38	Rhodamine 6G	2-Me THF/H_2O	Cs_2CO_3	24	39
39	Basic fuchsin	2-Me THF/H_2O	Cs_2CO_3	24	41

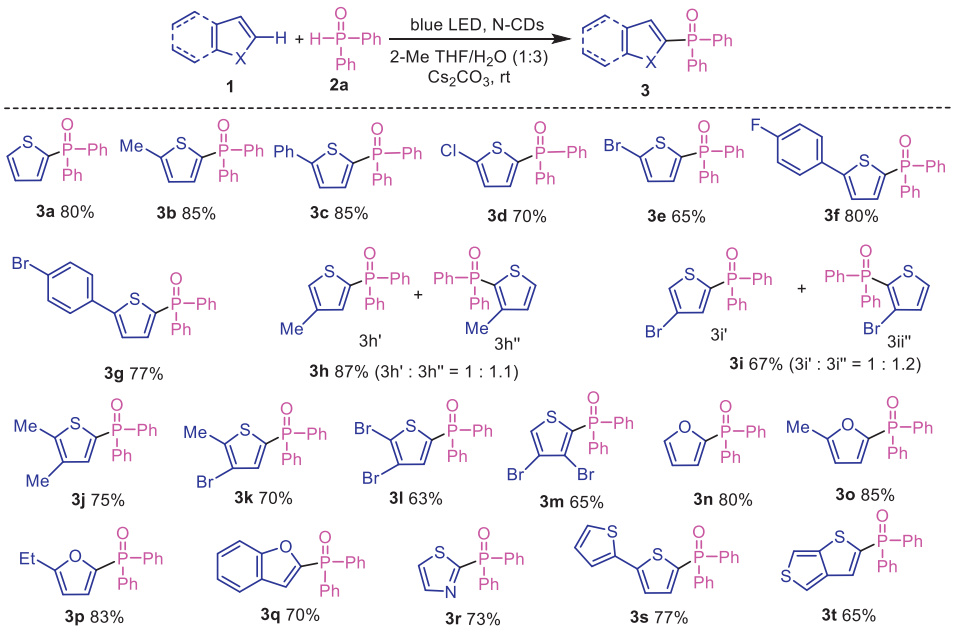
[a] Reaction conditions: diphenylphosphine oxide (1 mmol), 2-methylthiophene (2.5 mmol), photocatalyst (20 mg), solvent (3 mL), under light irradiation (10 W) at room temperature unless otherwise noted.
[b] Isolated yield.
[c] Red light.
[d] Green light.
[e] White light.
[f] Dark.
[g] N-CDs (10 mg).
[h] N-CDs (25 mg).

3-substituted thiophene is used as the substrate, a mixture of 2- and 5-phosphorylated products (**3h** and **3i**) is formed. The disubstituted thiophenes also proved themselves as excellent partners, smoothly coupling to generate the target products (**3j**-**3m**) with satisfactory yield. However, the reaction of diphenylphosphine oxide with some thiophene with hydroxyl and amine groups on ring failed to give the expected product.

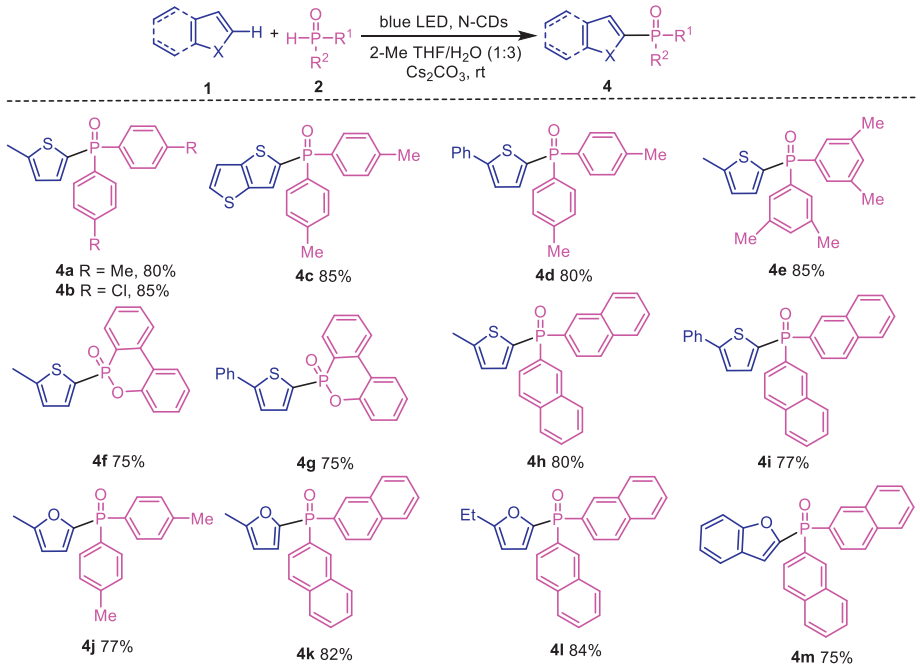
To put the versatility of this phosphonation process to an even tougher test, furan substrates took the stage. When reacted with diphenylphosphine oxide, they did not disappoint, delivering the corresponding products in high yields. Moreover, benzofuran is also a suitable substrate. Under the established reaction conditions, it delivered the expected phosphorylated product **3q** with a yield of 70%. 1,3-Thiazole can also participate in this reaction to present the expected product **3r** with a yield of 73%. When it came to 2,2′-bithiophene and thieno[2,3-*c*]thiophene, these double-thiophene-containing substrates, the reaction was highly selective. They only selectively produce single phosphorylation products **3s** and **3t**. No difunctional byproducts dared to show up, making the reaction a clean and precise operation. However, not all heteroaryl compounds exhibit compatibility with this photocatalytic system. Specifically, nitrogen-containing heterocycles (*e.g.*, indole and pyrrole) fail to undergo effective phosphorylation under the optimized reaction conditions. A plausible rationale for this inactivity lies in their intrinsic structural and electronic properties. The active N-H moieties and electron-rich aromatic scaffolds of these heterocycles are hypothesized to impose a kinetic barrier that inhibits their engagement in the specific reaction pathway of the photocatalytic system. Furthermore, the bond dissociation energy of the expected reaction site of C(sp^2)-H donors exerted significant influence on the phosphorylation. This energy mismatch dictates that the reaction would require overcoming an excessively high activation energy barrier to proceed, thereby precluding efficient transformation. Additionally, in this protic solvent systems, the N-H bonds of indole and pyrrole are prone to protonation. This protonation event reduces the electron density of the aromatic system, which further diminishes the reactivity of these heterocycles toward the phosphorylation process.

Building upon the established optimal reaction conditions, a systematic investigation into the reactivity of diarylphosphine oxides was subsequently carried out. The detailed outcomes of this exploration are comprehensively summarized in Scheme 4. Diarylphosphine oxides, specifically 2-diphenyl phosphine oxides, featuring diverse substituents on the phenyl moiety, demonstrated remarkable reactivity. These compounds engaged in smooth chemical interactions with thiophene and furan, leading to the successful synthesis of the corresponding products. The yields of these reactions spanned a range from moderate to excellent, indicating the robustness and efficiency of the reaction system. Notably, cyclic phosphate esters emerged as highly reactive substrates within this reaction framework. They readily underwent the phosphorylation reaction, undergoing a chemical transformation that efficiently converted them into the desired products (**4f** and **4g**). The high-yield formation of these products underscores the unique reactivity profile of cyclic phosphate esters under the specified reaction conditions, highlighting their potential for further exploitation in related synthetic endeavors. Furthermore, substrates incorporating a naphthyl group also displayed favorable reactivity characteristics. The successful formation of products from these naphthyl-containing substrates provides additional compelling evidence for the broad substrate scope and general applicability of the developed protocol. This finding not only expands the range of viable substrates but also reinforces the reliability and versatility of the established reaction conditions for the phosphorylation of various phosphorus-containing compounds.

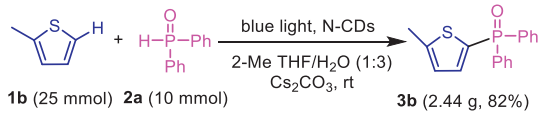
To assess the practical applicability and scalability of the developed synthetic methodology, a gram-scale reaction was conducted. Specifically, 2-methylthiophene (25 mmol) and diphenylphosphine oxide (10 mmol) were employed as reactants, and the reaction was executed under the optimized conditions. Upon completion of the reaction, the target product **3b** was isolated, yielding a separation yield of 82%. This result was in remarkable accordance with the findings obtained from the small-scale experiments, as vividly illustrated in Scheme 5. The close correspondence between the yields of the gram-scale and small-scale reactions not only validates the robustness and reliability of the developed protocol but also demonstrates its potential for industrial-scale applications. It provides compelling evidence that the synthetic approach can maintain consistent performance and efficiency even when the reaction scale is significantly increased, which is of great significance for the practical implementation of this methodology in both academic research and industrial production settings.



Scheme 3. Substrate scope for heteroaryl compounds with diphenylphosphine oxide. Reaction conditions: Diphenylphosphine oxide (1 mmol), heteroaryl compounds (2.5 mmol), Cs_2CO_3 (1 mmol), N-CDs (20 mg), and 2-Me THF/H_2O (1/3, 3 mL) under blue light irradiation at room temperature, 24 h, isolated yield.



Scheme 4. Substrate scope for substituted diphenyl phosphine oxides. Heteroaryl compound (2.5 mmol), substituted diphenylphosphine oxide (1 mmol), N-CDs (20 mg), Cs_2CO_3 (1 mmol), and 2-Me THF/H_2O (1:3, 3 mL) under blue light irradiation at room temperature, 24 h, isolated yield.



Scheme 5. Gram-scale synthesis **3b**

In the context of sustainable chemical synthesis, both economic viability and environmental friendliness are of paramount importance. The reusability and stability of photocatalysts serve as crucial metrics for evaluating their catalytic performance and determining their potential for practical applications. To comprehensively assess these aspects of N-CDs, a model reaction involving 2-methylthiophene and diphenylphosphine oxide was carried out under the previously established reaction conditions. Upon completion of the reaction, the mixture was extracted with ethyl acetate and water, N-CDs were in the water layer and the product was in the ethyl acetate layer. The water layer containing N-CDs was collected and dialyzed with deionized water for 24 h. After being dried, the recovered N-CDs were employed in ten consecutive reaction cycles. The experimental results demonstrated an exceptional level of catalytic stability, as no significant decline in catalytic efficiency was observed for seven additional cycles (Fig. 7).

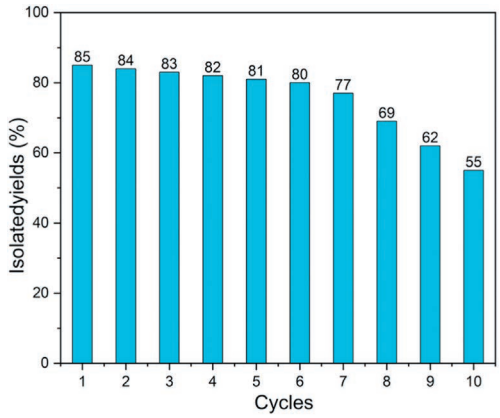


Fig. 7. Recyclability of N-CDs for the model reaction.

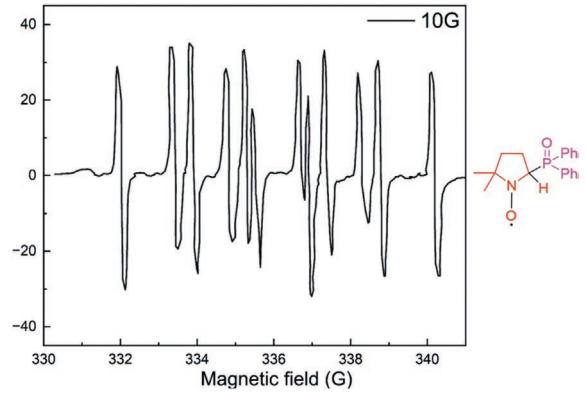
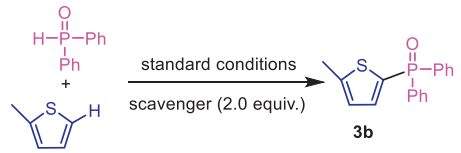
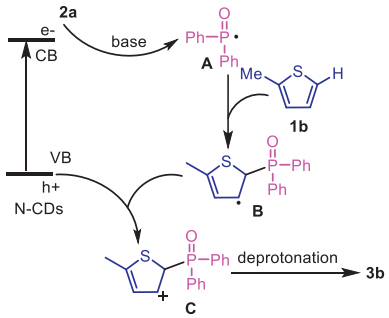


Fig. 8. EPR signals of the reaction solution in the presence of DMPO as spin-trapping reagents.



Scavenger	Inhibited species	Yield (%)
$CuCl_2$	SET	12%
$K_2S_2O_8$	electron scavenger	8%
TEOA	hole	11%
ferrocene	hole	12%
TEMPO	radical	15%
1,1-diphenylethylene	radical	6%
N_2		82%

Scheme 6. Control experiments.



Scheme 7. Proposed reaction mechanism.

However, it was observed that after the eighth cycle, the yield of isolated product gradually decreased. The decrease of yield can be attributed to the loss of catalyst in the recovery process. Moreover, the structural integrity of N-CDs was further investigated. FTIR and TEM analyses (Figs. 2 and 4) provided conclusive evidence that both the morphology and structure of N-CDs remained essentially unaltered even after the fifth reuse cycle. These findings not only highlight the remarkable reusability of N-CDs but also underscore their outstanding stability, thereby firmly supporting the potential of N-CDs as a promising photocatalyst for various catalytic transformations.

Investigation of the reaction mechanism was conducted through systematic control experiments. The absence of catalytic activity upon introduction of $CuCl_2$, a single-electron transfer (SET) quencher, suggested potential involvement of radical-mediated SET processes. Suppression of reaction efficiency was observed following addition of electron scavengers ($K_2S_2O_8$) and hole scavengers (TEOA and ferrocene), confirming the necessity of both charge carriers in the transformation sequence. In addition, the reaction inhibition was observed with 2,2,6,6-tetramethylpiperidin-1-oxy (TEMPO) and 1,1-diphenylethylene, two distinct radical trapping agents. Notably, the product **3b** can be successfully formed in nitrogen atmosphere, indicating that oxygen is not essential for this reaction (Scheme 6). Meanwhile, high-resolution mass spectrometry (HRMS) identified a 1,1-diphenylethylene-adducted intermediate species. Besides, electron spin resonance (ESR) spectroscopy detected a P-centered radical species was observed by using 5,5-dimethyl-1-pyrroline *N*-oxide (DMPO) as spin-trapping reagent (Fig. 8) [68]. Cumulative evidence from these complementary technologies confirms that this photoinduced reaction proceeded *via* a radical pathway.

On the basis of the above experiments, a plausible mechanism pathway for this photoinduced phosphorylation is proposed (Scheme 7). Under visible light irradiation, N-CDs are excited, generating holes (h^+) in the valence band (VB) and photogenerated electrons (e^-) in the conduction band (CB), thus forming electron-hole pairs. The holes in the VB of N-CDs possess strong oxidizing properties and can abstract one electron from the diphenylphosphine oxide (**2b**) molecule. This induces a single-electron oxidation of diphenylphosphine oxide, leading to the formation of P-centered radicals (**A**). The generated P-centered radicals (**A**), acting as active species, undergo a nucleophilic addition reaction with 2-methylthiophene (**1b**). They attack the sites with high electron cloud density in the 2-methylthiophene molecule, resulting in the formation of a radical intermediate (**B**). The remaining holes in the VB of N-CDs abstract one electron from the radical intermediate **B**. This causes further oxidation of intermediate **B**, which is then converted into a carbocation intermediate (**C**). The carbocation intermediate (**C**) undergoes a deprotonation reaction, losing one proton (H^+) to be converted into the target phosphorylated product (**3b**). Meanwhile, the hydrogen radicals ($H\cdot$) generated by dissociation in the reaction process combine with each other and undergo a coupling reaction to form hydrogen gas (H_2) as a by-product.

A comparative analysis of the developed catalytic system and previously reported methodologies for the model reaction is presented in Table 2. Notably, the proposed approach employs metal-free carbon dots as the photocatalyst, with the reaction conducted in a tetrahydrofuran/water (2-Me THF/H_2O) mixed solvent system. This configuration offers a greener alternative to the metal-based catalysts and toxic organic solvents utilized in earlier studies. Under mild reaction conditions, the developed catalytic system achieves efficient substrate conversion while sustaining a high target product yield. Distinct from previously reported catalytic systems featuring non-recoverable catalysts, the strategy proposed herein effectively addresses this critical limitation through catalyst recyclability. Additionally, the utilization of low-cost CDs min-

Table 2
Comparison of this catalytic system with the reported methods.

Entry	Reaction condition	Ref.
1	(+) Carbon rod Pt(-), 7.5 mA, N_2, 80 °C, $Mn(OAc)_2{\cdot}3H_2O$, 1,10-phen·H_2O, $^nBu_4NBF_4$, HOAc, 4 h, 81 %	[33]
2	$Co(dmgH)_2pyCl$, pyridine, N_2, blue LEDs, r.t. in DCM, 24 h, 62 %	[38]
3	$Co(dmgH)_2pyCl$, triethylamine, N_2, blue LEDs, r.t. in DCM, 36 h, 62 %	[39]
4	N-CDs, Cs_2CO_3, blue LEDs, r.t. in 2-Me THF/H_2O, 24 h, 85 %	This work

imizes material reduces the overall operational cost of the reaction process. Beyond simplifying the synthetic protocol, the developed method aligns with the core principles of green chemistry, as it minimizes waste generation, lowers energy consumption, eliminates the use of harmful organic solvents, and obviates the requirement for electrochemical equipment. Furthermore, in comparison with prior works [38,39], *E*-factor has been greatly improved from 3.30 to 0.76 (for detailed information, see Supporting information).

In this study, we report a groundbreaking advancement in the field of photocatalysis, wherein carbon quantum dots (CQDs) are employed for the first time as efficient photocatalysts. Under ambient temperature conditions, these CQDs enable the direct dehydrogenative C-H phosphinoylation of a wide array of heteroaryl compounds with various H-phosphine oxides. This catalytic protocol provides a straightforward and efficient synthetic route to access a diverse library of heteroaryl organophosphorus compounds, which are of significant importance in organic synthesis, materials science, and medicinal chemistry. One of the notable features of this newly developed methodology is its scalability. The reaction can be readily adapted for gram-scale synthesis, facilitating potential industrial applications. Additionally, the utilization of a 2-methyltetrahydrofuran/water mixture as the reaction solvent not only promotes the reaction efficiency but also aligns with the principles of green chemistry by reducing the environmental impact associated with the use of conventional organic solvents. The designed CQDs exhibit remarkable reusability, maintaining their catalytic activity over seven consecutive reaction cycles without significant loss of efficiency. This outstanding recyclability, coupled with their low cost and non-toxic nature, highlights the potential of CQDs as promising alternatives to expensive metal-based catalysts and organic dyes in photo-driven organic reactions. The present work not only expands the application scope of carbon quantum dots in photocatalysis but also paves the way for the development of more sustainable and cost-effective synthetic strategies in the realm of organic transformations.

Declaration of competing interest

The authors declare that they have no known competing financial interests or personal relationships that could have appeared to influence the work reported in this paper.

CRediT authorship contribution statement

Tong Yue: Methodology, Data curation, Conceptualization. **Jun-Bo Wang:** Data curation. **Xin-Yue Wang:** Data curation. **Ming-Yi Huang:** Data curation. **Mo Zhang:** Writing – original draft, Funding acquisition. **Zhan-Hui Zhang:** Writing – review & editing, Project administration, Funding acquisition, Conceptualization.

Acknowledgments

The authors gratefully acknowledge financial support for this work by Hebei Education Department (No. JZX2024004), the National Natural Science Foundation of China (No. 22301060), Central Guidance on Local Science and Technology Development Fund of Hebei Province (No. 236Z1404G), China Postdoctoral Science Foundation (No. 2023M730914) and Project of Science and Technology Department of Hebei Province (No. 22567622H).

Supplementary materials

Supplementary material associated with this article can be found, in the online version, at doi:10.1016/j.cclet.2025.112050.

References

[1] T.T. Fu, H.W. Qiao, Z.M. Peng, et al., Org. Biomol. Chem. 12 (2014) 2895–2902.
[2] L.H. Hong, W.J. Feng, W.C, et al., Dalton Trans. 52 (2023) 5101–5109.
[3] J. Xu, P.B. Zhang, Y.Z. Gao, et al., J. Org. Chem. 78 (2013) 8176–8183.
[4] H. McErlain, L.M. Riley, A. Sutherland, J. Org. Chem. 86 (2021) 17036–17049.
[5] M.B. Kurosawa, R. Isshiki, K. Muto, J. Yamaguchi, J. Am. Chem. Soc. 142 (2020) 7386–7392.
[6] R. Isshiki, K. Muto, J. Yamaguchi, Org. Lett. 20 (2018) 1150–1153.
[7] T. Wang, S. Sang, L. Liu, et al., J. Org. Chem. 79 (2014) 608–617.
[8] G.F. Zhang, J. Wang, C.F. Guan, et al., Eur. J. Org. Chem. 2021 (2021) 810–813.
[9] J.Y. Dong, L. Liu, X.Y. Ji, et al., Org. Lett. 21 (2019) 3198–3203.
[10] T.Q. Chen, J.S. Zhang, L.B. Han, Dalton Trans. 45 (2016) 1843–1849.
[11] D. Saha, T. Kaur, A. Sharma, Asian J. Org. Chem. 5 (2016) 1280–1287.
[12] C.D. Hou, Y.L. Ren, R. Lang, et al., Chem. Commun. 48 (2012) 5181–5183.
[13] M. Gao, Y. Li, L.J. Xie, et al., Chem. Commun. 52 (2016) 2846–2849.
[14] H.J. Zhang, W.D. Lin, Z.J. Wu, et al., Chem. Commun. 51 (2015) 3450–3453.
[15] Y.F. Wang, Y.J. Yang, K. Jie, et al., ChemCatChem 10 (2018) 716–719.
[16] Y. Yu, Z.B. Yue, L.G. Ding, et al., ChemistrySelect 4 (2019) 1117–1120.
[17] T. Kittikool, K. Phakdeeyothin, T. Chantarojsiri, S. Yotphan, Eur. J. Org. Chem. 2021 (2021) 3071–3078.
[18] N. Sabat, L.P. Slavetínská, B. Klepetárová, M. Hocek, J. Org. Chem. 81 (2016) 9507–9514.
[19] S.P. Archna, P.A. Chawla, Bioorg. Chem. 101 (2020) 104026.
[20] N.V. Bhilare, P.B. Auti, V.S. Marulkar, V.J. Pise, Mini-Rev. Med. Chem. 21 (2021) 217–232.
[21] Q.H. Liu, S.L. Kang, Z.S. Cui, et al., Green Chem. 26 (2024) 4803–4810.
[22] M.V. Stambirskyi, T. Kostiuk, S.I. Sirobaba, et al., J. Org Chem. 86 (2021) 12783–12801.
[23] Q. Dang, S.R. Kasibhatla, W. Xiao, et al., J. Med Chem. 53 (2009) 441–451.
[24] S. Ryu, P.G. Kim, M. Son, et al., Synth. Met. 301 (2024) 117538.
[25] S. Cauteruccio, D. Dova, M. Benaglia, et al., Eur. J. Org. Chem. 2014 (2014) 2694–2702.
[26] H.L. Mu, J.H. Ye, G.L. Zhou, et al., Chin. J. Polym. Sci. 38 (2019) 579–586.
[27] J. Ohshita, Y. Kurushima, K.H. Lee, et al., Organometallics 26 (2007) 6591–6595.
[28] T. Benincori, S. Gladiali, S. Rizzo, F. Sannicolò, J. Org. Chem. 66 (2001) 5940–5942.
[29] P. Zhang, Y.A. Wang, Z.X. Deng, J.T. Gao, Org. Biomol. Chem. 23 (2025) 546–578.
[30] X.J. Mu, J.P. Zou, Q.F. Qian, W. Zhang, Org. Lett. 8 (2006) 5291–5293.
[31] S. Hore, A. Srivastava, R.P. Singh, J. Org. Chem. 84 (2019) 6868–6878.
[32] O. Berger, J.L. Montchamp, Chem. Eur. J. 20 (2014) 12385–12388.
[33] S.Y. Wang, Q.L. Xue, Z.P. Guan, et al., ACS Catal. 11 (2021) 4295–4300.
[34] F.L. Zeng, Z.H. Jia, T.P. Loh, Adv. Synth. Catal. 366 (2024) 4536–4547.
[35] R. Wang, X. Liu, H. Hou, M.F. Zheng, ChemCatChem 17 (2025) e202401842.
[36] P.C. Cui, Z.C. Yin, G.W. Wang, Org. Lett. 25 (2023) 2663–2668.
[37] S.P.M. Ung, V.A. Mechrouk, C.J. Li, Synthesis 53 (2021) 1003–1022.
[38] A.L. Shao, J.F. Chen, L.X. Wang, et al., Org. Chem. Front. 9 (2022) 4379–4387.
[39] J.X. Yu, Y.Y. Cheng, C. Bin, et al., Angew. Chem. Int. Ed. 61 (2022) e202209293.
[40] Y. Wang, Y. Liu, X. Duan, et al., Chem. Soc. Rev. 54 (2025) 2436–2482.
[41] C. Xie, Z.W. Jiang, Y.Y. Pang, et al., Green Chem. 26 (2024) 6886–6899.
[42] A. Bahuguna, A. Kumar, V. Krishnan, Asian J. Org. Chem. 8 (2019) 1263–1305.
[43] A. Carioscia, E. Cocco, M.E. Casacchia, et al., ACS Catal. 14 (2024) 13429–13438.
[44] C. Rosso, G. Filippini, M. Prato, ACS Catal. 10 (2020) 8090–8105.
[45] P. Wang, C.M. Chen, H.W. Ren, E.R. Duan, Chin. Chem. Lett. 36 (2025) 110725.
[46] V. Corti, B. Bartolomei, M. Mamone, et al., Eur. J. Org. Chem. 2022 (2022) e202200879.
[47] B.B. Chen, M.L. Liu, C.Z. Huang, Green Chem. 22 (2020) 4034–4054.
[48] Y.L. Hu, O. Seivert, Y. Tang, et al., Angew. Chem. Int. Ed. 63 (2024) e202412341.
[49] D. Saini, A.K. Garg, C. Dalal, et al., ACS Appl. Nano Mater. 5 (2022) 3087–3109.
[50] F.Y. Villanueva, J. Manioudakis, R. Naccache, M.B. Majewski, ACS Appl. Nano Mater. 3 (2020) 2756–2765.
[51] I.N. Chakraborty, P. Roy, P.P. Pillai, ACS Catal. 13 (2023) 7331–7338.
[52] Y.Z. Han, H. Huang, H.C. Zhang, et al., ACS Catal. 4 (2014) 781–787.
[53] D. Sarma, B. Majumdar, T.K. Sarma, ACS Sustainable Chem. Eng. 6 (2018) 16573–16585.
[54] Y. Yu, Q.S. Zeng, S.Y. Tao, et al., Adv. Sci. 10 (2023) 2207621.
[55] M. Sbacchi, M. Mamone, L. Morbiato, et al., ChemCatChem 15 (2023) e202300667.
[56] K.K. Niu, R.Z. Zhang, X.Z. Yang, et al., ChemCatChem 17 (2024) e202301686.
[57] S. Cailotto, M. Negrato, S. Daniele, et al., Green Chem. 22 (2020) 1145–1149.
[58] C. Campalani, M. Durai, W. Leitner, A. Bordet, Green Chem. 27 (2025) 2666–2671.

[59] M. Jouyandeh, S.S.M. Khadem, S. Habibzadeh, et al., Green Chem. 23 (2021) 4931–4954.
[60] S. Paul, S. Panja, N. Hazra, et al., J. Org. Chem. 89 (2023) 91–100.
[61] T.T. He, H.P. Wei, Y.B. Zhou, et al., Org. Chem. Front. 10 (2023) 2918–2926.
[62] S.L. Kang, T. Yue, Z.H. Zhang, et al., ACS Sustainable Chem. Eng. 12 (2024) 18200–18210.
[63] J.B. Wang, T. Yue, Z.H. Zhang, et al., Green Chem. 26 (2024) 12034–12042.
[64] Y. Guan, Y.L. Ying, Z.H. Zhang, et al., J. Catal. 443 (2025) 115938.
[65] W.J. Li, J.B. Wang, Z.H. Zhang, et al., Chin. Chem. Lett. 36 (2025) 110001.
[66] W.J. Li, Z.Q. Wang, J.B. Wang, et al., J. Catal. 430 (2024) 115308.
[67] Y. Guan, B. Wang, Y.L. Ying, P. Li, Z.H. Zhang, Green Chem. 27 (2025) 9165.
[68] Z.J. Li, F.H. Fan, Z.Y. Zhang, et al., RSC Adv. 5 (2015) 27853–27856.